

Meter-baseline tests of sterile neutrinos at Daya Bay

Y. Gao¹ and D. Marfatia²

¹*Department of Physics, University of Oregon, Eugene, OR 97403, U.S.A.*

²*Department of Physics and Astronomy, University of Kansas, Lawrence, KS 66045, U.S.A.*

We explore the sensitivity of an experiment at the Daya Bay site, with a point radioactive source and a few meter baseline, to neutrino oscillations involving one or more eV mass sterile neutrinos. We find that within a year, the entire 3+2 and 1+3+1 parameter space preferred by global fits can be excluded at the 3σ level, and if an oscillation signal is found, the 3+1 and 3+2 scenarios can be distinguished from each other at more than the 3σ level provided one of the sterile neutrinos is lighter than 0.5 eV.

Introduction. The standard three neutrino (3ν) picture has been successful in explaining most oscillation data. However, data from the Liquid Scintillator Neutrino Detector (LSND) experiment [1] when interpreted as arising from $\bar{\nu}_\mu \rightarrow \bar{\nu}_e$ oscillations, indicate a deviation from the simple 3ν picture. The Mini-Booster Neutrino Experiment (MiniBooNE) [2] provides supporting evidence for the LSND result that oscillations involving an eV mass sterile neutrino may be at work. Additional support may be found in an upward revision in the estimate of the reactor $\bar{\nu}_e$ flux yield [3]. The fact that short baseline (SBL) reactor neutrino experiments do not detect the 3% larger flux (via a 7% larger event rate) could be explained as a consequence of oscillations to sterile states.

Popular scenarios that are consistent with the the relevant data have either one sterile neutrino, with a 3+1 mass spectrum (such that the nearly degenerate triplet of mass eigenstates is lighter than the remaining state), or 2 sterile neutrinos [4, 5]. The 5 neutrino (5ν) case has 2 viable spectra: a 3+2 spectrum in which the triplet is lighter than both sterile neutrinos, and a 1+3+1 spectrum in which one sterile neutrino is lighter than the triplet and one is heavier. In all cases, the sterile neutrinos mix little with the active neutrinos.

Recently, it was suggested that a ten kilocurie scale ^{144}Ce - ^{144}Pu β -decay source could be placed inside a large liquid scintillator detector to study eV sterile neutrino oscillations on baselines of a few meters with 1.8-3.3 MeV neutrinos [6]. Distinct virtues of this technique are (1) that with a point-like source, an oscillation signature can be demonstrated as a function of both energy and baseline, (2) the short baseline may be easily adjustable, (3) existing detectors can be utilized, and (4) antineutrino source activity is reduced relative to that of neutrino sources previously used for the calibration of low-energy radiochemical solar neutrino experiments since the inverse beta-decay cross section is higher than the neutrino-electron scattering cross section. Clear technical challenges are the feasibility of constructing such an intense radioactive source and of engineering suitable ultra-pure shielding of the source inside the detector. For

a decisive measurement, Ref. [7] considered the possibility of an experiment at the Daya Bay site with a 500 kCi (1.85×10^{16} Bq) source. The configuration of the 4 detectors in the Far Hall at Daya Bay makes it possible to place the source outside the detectors thus circumventing one of the technical issues. We treat the 500 kCi source as point-like although it will have a finite spatial extent depending on the freshness of the fuel being used for its production, the production and transportation time, as well as the final density of cerium oxide that is limited to about 4.5 g/cm^3 . This approximation is valid since the size of the source will be small compared to the 6.5 m oscillation length of interest.

In this Letter we show that the parameter space preferred by global fits in the 3+1, 3+2 and 1+3+1 scenarios will be stringently tested by the proposed multi-meter baseline $\bar{\nu}_e$ disappearance measurement at Daya Bay. For sterile neutrino masses below 0.5 eV, such a measurement can even distinguish between the 3+1 and 3+2 scenarios at the 3σ level. This enhanced sensitivity arises because knowledge of the ν_e fraction of the ν_4 and ν_5 mass eigenstates breaks the degeneracy in the sterile mixings to ν_e and ν_μ , both of which are required to explain the anomalous SBL data.

Sterile neutrino oscillations. For vacuum oscillations of MeV neutrinos from a radioactive source, the (CP phase-independent) ν_e and $\bar{\nu}_e$ survival probability at distance L is

$$P_{ee} = 1 - 4 \sum_{i < j} |U_{ei}|^2 |U_{ej}|^2 \sin^2 \Delta_{ij}, \quad (1)$$

where $\Delta_{ij} = \delta m_{ij}^2 L / (4E_\nu)$ with $\delta m_{ij}^2 = m_i^2 - m_j^2$. i, j denote the mass eigenstates and take values from 1 to the total number of neutrinos. U_{ei} are elements of the mixing matrix. For the 3+1 spectrum, $\delta m_{43}^2 \simeq \delta m_{42}^2 \simeq \delta m_{41}^2 \simeq 1 \text{ eV}^2 \gg \delta m_{32}^2 \simeq \delta m_{31}^2 \simeq 2.4 \times 10^{-3} \text{ eV}^2 \gg \delta m_{21}^2 \simeq 7.5 \times 10^{-5} \text{ eV}^2$. Then, $P_{ee}^{3+1} = 1 - \sin^2 2\theta_s \sin^2 \Delta_{41}$, with the definition, $\sin \theta_s \equiv U_{e4}$.

In the 5ν case, Eq. (1) includes a superposition of three oscillation frequencies corresponding to $\delta m_{41}^2, \delta m_{51}^2$ and δm_{54}^2 . We neglect the δm_{54}^2 contribution in what follows. Although the sterile neutrinos can mix with all three ac-

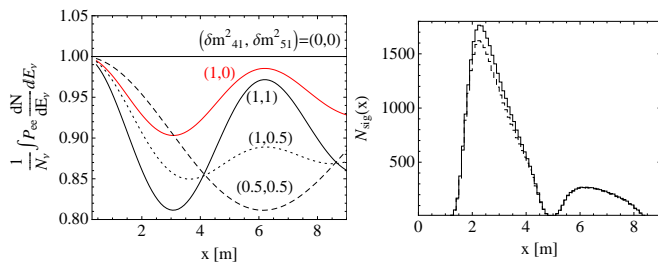


FIG. 1. Left: The energy-averaged ν_e survival probability as a function of distance for 3+1 and 3+2 sample points. $U_{e4} = 0.16$ (giving a $\sim 10\%$ oscillation amplitude), and in the 3+2 scenario, U_{e5} is also 0.16. Right: Event distributions for the chosen radioactive source-detector configuration. The solid and dashed curves show the cases of no active-sterile oscillations [7], and of oscillations with $\delta m^2 = 1 \text{ eV}^2$ and a 10% oscillation amplitude, respectively.

time neutrinos, P_{ee} depends only on the four parameters, $\delta m_{41}^2, \delta m_{51}^2, |U_{e4}|$ and $|U_{e5}|$ via

$$P_{ee}^{5\nu} = 1 - 4(1 - |U_{e4}|^2 - |U_{e5}|^2) \times (|U_{e4}|^2 \sin^2 \Delta_{41} + |U_{e5}|^2 \sin^2 \Delta_{51}). \quad (2)$$

Since $P_{ee}^{5\nu}$ is insensitive to the signs of Δ_{41} and Δ_{51} , ν_e disappearance data cannot distinguish between the 3+2 and 1+3+1 spectra for identical mixing matrix elements. (In principle, the spectra can be distinguished if the suppressed but nonzero δm_{54}^2 contribution to the right hand side, $-4|U_{e4}|^2|U_{e5}|^2 \sin^2 \Delta_{54}$, is included.)

In the left panel of Fig. 1, we show the ν_e survival probability for several 3+1 and 3+2 sample points. For the sake of illustration, we have used somewhat large values of U_{e4} and U_{e5} . The significant variation in the survival probabilities over the first few meters for different $(\delta m_{41}^2, \delta m_{51}^2)$ choices reveals the strength of the method. For all curves in Fig. 1, P_{ee} is convolved with the $\bar{\nu}_e$ energy spectrum from the radioactive source.

Experimental set-up and procedure. The 500 kCi radioactive source at Daya Bay can be placed so that the 4 cylindrical detectors collect $\bar{\nu}_e$ data with baselines from 1 to 8 meters. Several possible source locations have been studied, each giving a different spatial coverage of $P_{ee}(L)$. We choose ‘‘Point B’’ in the jargon of Ref. [7], which is located halfway between two of the detectors, and samples 2 principal baselines. It provides superior sensitivity for $\delta m^2 \sim 1 \text{ eV}^2$ with an oscillation length of about 6.5 meters. The no oscillation signal event rate is about 38,000 in one year after accounting for the 66.3% decrease in source activity over a one-year period [7]. Event distributions as a function of baseline are shown in the right panel of Fig. 1; the detector energy and position resolutions are $9\%/\sqrt{E(\text{MeV})}$ and 15 cm, respectively [7]. Depending on the energy window used, the reactor neutrino background is expected to lie between 22,000-32,000 events per year. However, this large background can be

controlled because its shape will be known.

We take the detectors to be identical and adopt the following χ^2 for our analysis [7]:

$$\chi^2 = \sum_{i,j} \frac{(N_{i,j}^{ex} - N_{i,j}^{th})^2}{N_{i,j}^{ex}(1 + \sigma_b^2 N_{i,j}^{ex})} + \left(\frac{\alpha_s}{\sigma_s}\right)^2 + \left(\frac{\alpha_r}{\sigma_r}\right)^2, \quad (3)$$

where $N_{i,j}^{ex}$ is a simulated dataset and $N_{i,j}^{th}$ is the theoretical expectation for a given set of oscillation parameters, and i and j run over position and visible energy bins, respectively. $\sigma_s = 0.01$ and $\sigma_r = 0.01$ are the normalization uncertainties in the signal and reactor background fluxes, respectively, and $\sigma_b = 0.02$ is the bin-to-bin uncertainty [7]. α_s and α_r are nuisance parameters that are allowed to float. N^{ex} and N^{th} are given by

$$N_{i,j}^{th/ex} = (1 + \alpha_s)\tilde{S}_{i,j}^{th/ex} + (1 + \alpha_r)\tilde{R}_{i,j}, \quad (4)$$

where \tilde{S} and \tilde{R} ($=28,000/\text{year}$) are the number of signal events from the source and the number of reactor background events, respectively.

The number of signal events (in all 4 detectors) with sterile neutrino oscillations is obtained by scaling the number of events for the 3ν case:

$$\tilde{S}_{i,j}^{th} = P_{ee}(L_i, E_\nu) S_{i,j}^{3\nu} \quad \text{with} \quad S_{i,j}^{3\nu} = N_{tot} \left. \frac{\Delta n}{\Delta E_{vis}} \right|_i \left. \frac{\Delta n}{\Delta L} \right|_j, \quad (5)$$

where $\Delta n/\Delta E_{vis}$ and $\Delta n/\Delta x$ are normalized event distributions binned in visible energy and position, respectively, and $N_{tot} = 38,000$ is the total number of events for the 3ν case in one year. The positron’s energy in an inverse neutron β -decay event is $E_\nu - (m_n - m_p)$. Subsequent pair annihilation in the scintillator produces visible energy,

$$E_{vis} = E_\nu - (m_n - m_p) + m_e \simeq E_\nu - 0.8 \text{ MeV}. \quad (6)$$

3+1. We checked that in the 3+1 scenario our procedure yields a 95% confidence level (C.L.) sensitivity that is comparable to that of Ref. [7] for $\delta m_{41}^2 < 2 \text{ eV}^2$. The oscillation amplitude that fits the global SBL data is given by

$$\sin^2 2\theta_{SBL} = 4|U_{e4}|^2|U_{\mu 4}|^2. \quad (7)$$

Daya Bay data could push $|U_{e4}|$ down far enough that the value of $|U_{\mu 4}|$ needed to obtain an amplitude that explains the SBL data could conflict with the current bound on $|U_{\mu 4}|$ shown in the left panel of Fig. 2.

Since a meter-baseline measurement at Daya Bay will be independent of the earlier data, it is reasonable to impose the constraint on $U_{\mu 4}$ as a prior. Then, Daya Bay can rule out most of the allowed region from a fit to LSND and MiniBooNE antineutrino data; see the right panel of Fig. 2.

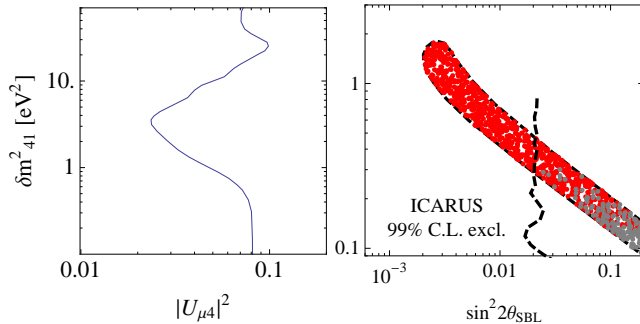


FIG. 2. A combination of the 99% C.L. bound on $|U_{\mu 4}|^2$ [8] from CDHS and atmospheric neutrino data (left) and a 99% C.L. null result at Daya Bay can rule out the red points of the 99% C.L. region favored by a joint analysis of LSND and Mini-BooNE antineutrino data in the 3+1 scenario [5] (right). The grey points survive the joint constraint, but not the ICARUS exclusion [9].

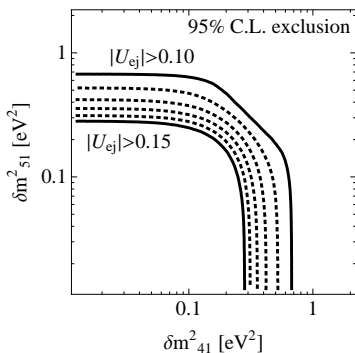


FIG. 3. 95% C.L. exclusion contours for the 5ν scenario, for $|U_{e 4}|$ and $|U_{e 5}|$ above $|U|_{min}$ in steps of 0.01. The region above each contour is excluded.

3+2 and 1+3+1. We first consider Daya Bay’s sensitivity to the 5ν scenario without recourse to specific points, models or fits. We employ a grid in the $(\delta m_{41}^2, \delta m_{51}^2, |U_{e 4}|, |U_{e 5}|)$ parameter space, place a prior on the size of the mixing, $\min(|U_{e 4}|, |U_{e 5}|) = |U|_{min}$ in steps of size 0.01 from 0.10 to 0.15, and suppose a null result at Daya Bay. The 95% C.L. sensitivity in the $(\delta m_{41}^2, \delta m_{51}^2)$ plane is shown in Fig. 3. As mentioned before, P_{ee} does not depend on the signs of the mass-squared differences. So the results of Fig. 3 apply to both the 3+2 and 1+3+1 spectra.

We now specialize to 5ν models that are consistent with global neutrino data. In Table I, we display Daya Bay’s sensitivity to several best-fit points to SBL data in the 5ν case assuming that no oscillations are seen in the Daya Bay dataset. These points would be completely excluded by Daya Bay because of their sizable $U_{e 4}$ and $U_{e 5}$.

To examine Daya Bay’s capability to probe the large 5ν

Parametrization	χ^2	δm_{41}^2	δm_{51}^2	$ U_{e 4} $	$ U_{e 5} $	$ U_{\mu 4} $	$ U_{\mu 5} $
KMS (3+2) [5]	62	0.47	0.87	0.128	0.138	0.165	0.148
KMS (1+3+1) [5]	68	-0.47	0.87	0.129	0.142	0.154	0.163
GL (3+2) [4]	78	0.9	1.61	0.13	0.13	0.14	0.078
MM NH (3+2)[10]	64	0.47	0.87	0.149	0.127	0.112	0.127
MM IH (3+2)[10]	80	0.9	1.61	0.139	0.122	0.138	0.107
MMS (3+2) [11]	55	0.89	1.76	0.15	0.07	0.15	0.15

TABLE I. χ^2 values for some global best-fit points (to data from SBL experiments), for a simulated dataset with no oscillations at Daya Bay. ‘MM NH/IH’ is the ‘minimal model (with normal/inverted 3ν mass hierarchy)’ of Ref. [10] and ‘MMS’ is the ‘minimal seesaw model’ of Ref. [11].

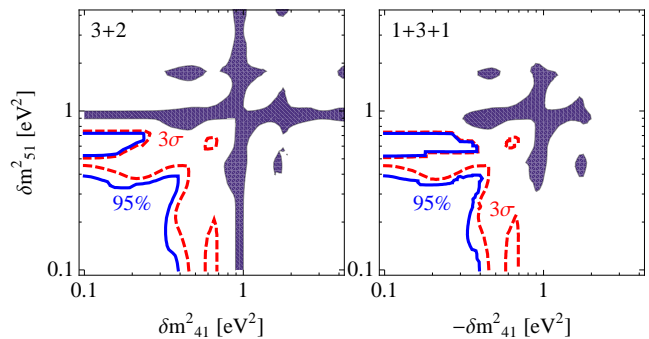


FIG. 4. The shaded regions are the 3σ globally preferred regions in the $(\delta m_{41}^2, \delta m_{51}^2)$ plane in the 3+2 (left) and 1+3+1 (right) scenarios [14]. A null result at Daya Bay can rule out the regions above the blue solid and red dashed contours at the 95% C.L. and 3σ , respectively. The exclusion regions are slightly different in the two panels because for each $(\delta m_{41}^2, \delta m_{51}^2)$, the best-fit mixing matrix elements from the fit of Ref. [14] are different for the two mass spectra.

parameter space, we use the globally allowed regions from an updated fit to the datasets listed in Ref. [5] in conjunction with data from the NOMAD [12] and CDHS [13] experiments [14]. The shaded areas of Fig. 4 are the globally allowed regions at 3σ . We see that at least one δm^2 is close to 1 eV^2 so as to explain the SBL data. All mixing parameters other than δm_{41}^2 and δm_{51}^2 are marginalized over and assume their best-fit values.

As the global fits favor significant $\bar{\nu}_\mu - \bar{\nu}_e$ transitions, the mixing parameters tend to be large enough to be testable at Daya Bay. Figure 4 shows that Daya Bay can exclude the 3+2 and 1+3+1 scenarios as an explanation of the LSND/MiniBooNE anomaly at 3σ .

3+1 or 3+2? So far we have demonstrated that a null result at Daya Bay can significantly constrain sterile neutrinos. We now entertain the possibility that future data confirms their existence. Then, a pressing issue will be to ascertain whether the 3+1 or the 3+2 scenario is operative. Since scenarios with more eigenstates should be able to mimic those with fewer eigenstates, a good

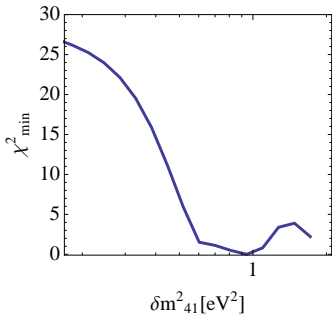


FIG. 5. The degree to which Daya Bay can discriminate between the 3+1 and 3+2 scenarios. We simulate an oscillation signal for points in the 99% C.L. region favored by LSND and MiniBooNE that are consistent with the 99% C.L. bound on $|U_{\mu 4}|$ (see Fig. 2), and fit the spectrum from points in the 3σ region of the 3+2 parameter space (see the left panel of Fig. 4) to the simulated data. A more than 3σ discrimination is possible for $\delta m^2_{41} < 0.5 \text{ eV}^2$.

test of Daya Bay’s discriminatory power is to fit 3+2 points to data simulated for 3+1. Assume that Daya Bay collects a dataset that is well-described by a point in the 3+1 parameter space. Then, in principle there is a 3+2 mixing scenario that gives the same oscillation pattern. However, this 3+2 point may be constrained by other oscillation data. To account for this possibility, we fit all the globally allowed 3+2 parameters to the 3+1 dataset and check if a good fit exists. The technical procedure is as follows.

For every point on a grid in the $(\delta m^2_{41}, \theta_{SBL}, |U_{e4}|)$ parameter space that lies within the 99% C.L. allowed region of the right panel of Fig. 2 and is also consistent with the 99% C.L. bound on $|U_{\mu 4}|$ in the left panel of Fig. 2, we simulate a dataset $N_{i,j}^{ex}$. We then fit points in 3+2 parameter space that are allowed at 3σ (shown in the left panel of Fig. 4) to this dataset (using Eq. 3), and find the 3+2 point with the minimum χ^2 corresponding to that $(\delta m^2_{41}, \theta_{SBL}, |U_{e4}|)$ point. For a given δm^2_{41} , we repeat the procedure for other values of $(\theta_{SBL}, |U_{e4}|)$ so

as to find the global χ^2_{min} for each δm^2_{41} . Note that the best-fit 3+2 value of δm^2_{41} need not be the same as the value for which 3+1 data was simulated.

We plot χ^2_{min} versus δm^2_{41} in Fig. 5. The discrimination between the 3+1 and 3+2 scenarios is better for small δm^2_{41} . This is because for small δm^2_{41} , the deviation of the 3+1 spectrum from the 3ν spectrum is small in the meter-baseline experiment, which is harder to replicate with a 3+2 point that must also reproduce the anomalous SBL data.

Acknowledgements. We thank V. Barger, K. Heeger and B. Littlejohn for discussions, and especially thank J. Kopp for providing us with data from the update to the fit of Ref. [5]. This work was supported by DOE Grants No. DE-FG02-04ER41308 and DE-FG02-96ER40969.

-
- [1] A. Aguilar-Arevalo *et al.*, Phys. Rev. D **64**, 112007 (2001) [hep-ex/0104049].
 - [2] A. A. Aguilar-Arevalo *et al.*, arXiv:1207.4809 [hep-ex].
 - [3] G. Mention, M. Fechner, T. Lasserre, T. A. Mueller, D. Lhuillier, M. Cribier and A. Letourneau, Phys. Rev. D **83**, 073006 (2011) [arXiv:1101.2755 [hep-ex]].
 - [4] C. Giunti and M. Laveder, Phys. Rev. D **84**, 073008 (2011) [arXiv:1107.1452 [hep-ph]].
 - [5] J. Kopp, M. Maltoni and T. Schwetz, Phys. Rev. Lett. **107**, 091801 (2011) [arXiv:1103.4570 [hep-ph]].
 - [6] M. Cribier *et al.*, Phys. Rev. Lett. **107**, 201801 (2011) [arXiv:1107.2335 [hep-ex]].
 - [7] D. A. Dwyer, K. M. Heeger, B. R. Littlejohn and P. Vogel, arXiv:1109.6036 [hep-ex].
 - [8] M. C. Gonzalez-Garcia and M. Maltoni, Phys. Rept. **460**, 1 (2008) [arXiv:0704.1800 [hep-ph]].
 - [9] M. Antonello *et al.*, arXiv:1209.0122 [hep-ex].
 - [10] A. Donini, P. Hernandez, J. Lopez-Pavon, M. Maltoni and T. Schwetz, JHEP **1207**, 161 (2012) [arXiv:1205.5230 [hep-ph]].
 - [11] J. Fan and P. Langacker, JHEP **1204**, 083 (2012) [arXiv:1201.6662 [hep-ph]].
 - [12] P. Astier *et al.*, Phys. Lett. B **570**, 19 (2003) [hep-ex/0306037].
 - [13] F. Dydak *et al.*, Phys. Lett. B **134**, 281 (1984).
 - [14] J. Kopp, private communication.